

Influence of Device Microstructure on The Optical Properties of Ge_{1-y}Sn_y ($y = 0-0.11$) LEDs Produced by Next Generation Deposition Methods.

J. D. Gallagher¹, T. Aoki², P. Sims³, J. Menendez¹, and J. Kouvetakis³

¹Department of Physics & Astronomy, Arizona State University, Tempe, AZ 85287 USA

²LeRoy Eyring Center for Solid State Science, Arizona State University, Tempe, AZ 85287 USA

³Department of Chemistry & Biochemistry, Arizona State University, Tempe, AZ 85287 USA

Ge_{1-y}Sn_y alloys represent a promising new class of IR semiconductors with tunable direct band gaps beyond that of Ge, allowing the optoelectronic capabilities of the material to be significantly extended into the mid IR. These alloys become direct gap semiconductors for $y = 0.09$ [1], making them an attractive alternative to Ge for application in purely group-IV interband lasers that are integrated onto Si-platforms. Significant progress has been made in recent years with the demonstration of high efficiency photodetectors and light emitting diodes containing up to 8% Sn [2,3]. However systematic optical studies of devices with concentrations near the indirect-to-direct transition are still lacking. A major problem with the synthesis of highly saturated materials with $y > 0.08$ is the strong dependence of the lattice parameter on the Sn content. This produces a significant lattice mismatch with Si and Ge platforms, making it difficult to integrate materials with sufficiently low defect densities as required for viable device performance. Furthermore, the associated compressive strains become an issue, rendering the material more indirect and adversely affecting light emission. For the fabrication of practical devices, relaxed films with large thickness are desirable but such films contain deleterious misfit dislocations that increase the non-radiative recombination rate. In this paper, we report the development of optimized growth protocols that enable fabrication of a new class of photodiodes featuring thick, bulk-like components with purposely designed microstructures. The device configurations comprise n -Ge/Ge_{1-y}Sn_y/ p -Ge_{1-y}Sn_y stacks grown directly upon Si(100). The constituent layers feature defect-engineered interfaces, allowing the fabrication of devices exhibiting strong direct-gap electroluminescence over a wide concentration range $0 \leq y \leq 0.11$ for the first time. The intrinsic active regions are grown largely relaxed on Ge-buffered Si following low-temperature routes based on specialty Ge₃H₈ and SnD₄ chemical sources. The devices contain only one defected interface between the intrinsic layer and the Ge buffer, while all other junctions are selected to be lattice-matched and thus devoid of dislocations.

Figure 1(a) is a Z-contrast image taken with a JEOL-ARM 200F showing the entire layer sequence of a sample comprising n -Ge, i -Ge, i -Ge_{0.895}Sn_{0.105} and p -Ge_{0.95}Sn_{0.05} components. The i -Ge layer in this case serves as a spacer between the bottom n -type contact and the active region to block threading dislocations from penetrating through. It also mitigates possible diffusion of the P dopants across the junction. All layers are highly uniform, exhibiting sharp and well-defined interfaces as required for effective device performance. Figure 1(b) is a XTEM image acquired on a JEOL-4000EX, showing a flat free surface and a defect-free top interface. The bottom interface is defected, as evidenced by the presence of multiple edge dislocations and dislocation loops confined to the plane of growth. The microstructure of the interfaces was further characterized by high resolution STEM, and representative BF images are shown in Figure 2(b,c) for Ge_{0.915}Sn_{0.085} and Ge_{0.895}Sn_{0.105} devices. The main types of defects accommodating the lattice mismatch are found to be 60° dislocations and short stacking faults originating at the interface and penetrating down into the lower energy Ge buffer. Higher defect densities are observed in the more concentrated alloy samples, as expected, leading to undesirable non-

radiative recombination, thus limiting the overall optical response. Figure 2(a) shows that in contrast to the bottom (*n-i*) interface, the top (*i-p*) counterpart is defect-free, thereby reducing non-radiative recombination in these devices. Figure 2(d) shows EL spectra vs composition for a representative set of samples across the entire 2-11% Sn composition range. Note that the emission intensities increase as a function of Sn, as expected due to the reduction of the direct-indirect edge separation. An anomaly to this trend is seen between the 2% Sn and 5.5% Sn plots in the Figure. This is attributed to an increase in non-radiative recombination as the mismatch strains between the device components in the 5.5% device partially relax via generation of misfit dislocations [4].

References:

- [1] J. D. Gallagher, *et al.*, Applied Physics Letters, **105** (2014), p. 142102.
 [2] H. H. Tseng, *et al.*, Applied Physics Letters, **102** (2013), p. 182106.
 [3] Wei Du, *et al.*, Applied Physics Letters, **104** (2014), p. 241110.
 [4] This work was supported by the NSF. We acknowledge the use of facilities at the John M. Cowley Center for High Resolution Electron Microscopy at Arizona State University.

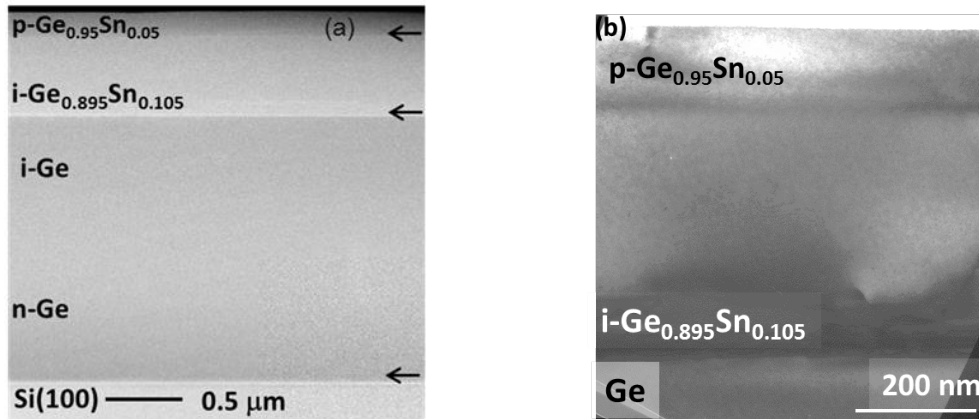


Figure 1. Panel (a) Z-contrast image of an entire device stack including the Si substrate. Panel (b) Diffraction contrast image showing the typical interface and bulk layer microstructure of the same device in low magnification.

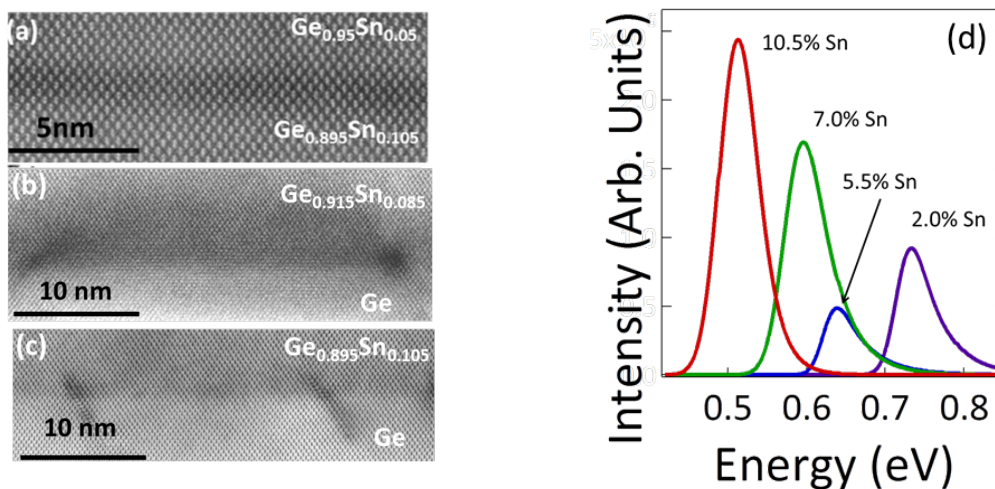


Figure 2 (a) STEM HAADF image shows no defects at the top *i-p* junction. (b,c) STEM BF micrographs of defective Ge/*i-Ge*_{0.915}Sn_{0.085} and Ge/*i-Ge*_{0.895}Sn_{0.105} interfaces. (d) EL spectra of Ge_{1-y}Sn_y heterostructure diodes. The plots represent EMG fits of the direct gap emission.